Effect of Si/Fe Composition, Substrate Temperature, and Substrate Orientation on the Structure and Magnetic Properties of Fe-Si Alloy Film

Takuya Aida[1], Tetsuroh Kawai[1], Mitsuru Ohtake[1,2], Masaaki Futamoto[1],
Fumiyoshi Kirino[3], and Nobuyuki Inaba[4]

[1]Faculty of Science and Engineering, Chuo University, *1-13-27 Kasuga, Bunkyo-ku, Tokyo 112-8551, Japan*
[2]Faculty of Engineering, Kogakuin University, *2665-1 Nakano, Hachioji, Tokyo 192-0015, Japan*
[3]Graduate School of Fine Arts, Tokyo University of the Arts, *12-8 Ueno-Koen, Taito-ku, Tokyo 110-8714, Japan*
[4]Faculty of Engineering, Yamagata University, *4-3-16 Jyonan, Yonezawa, Yamagata 992-8510, Japan*

$Fe_{100-x}Si_x$ (x = 0, 2, 6, 10 at. %) alloy films are prepared on MgO single-crystal substrates of (001), (110), and (111) orientations at temperatures ranging between room temperature and 600 °C by using a radio-frequency magnetron sputtering system. The film growth behavior, the crystallographic properties, and the magnetic properties are systematically investigated. Fe-Si(001) single-crystal films with bcc structure are formed on MgO(001) substrates. The Fe-Si films deposited on MgO(110) substrates consist of epitaxial bcc(211) bi-crystals whose orientations are rotated around the film normal by 180° each other. Fe-Si films grow epitaxially on MgO(111) substrates with two types of bcc(110) variant whose crystallographic orientations are similar to the Nishiyama-Wasserman and the Kurdjumov-Sachs relationships. The orientation dispersion of Fe-Si film decreases with decreasing the Si composition, with increasing the substrate temperature, and with decreasing the index of the substrate crystallographic plane. The Fe-Si films deposited on MgO(001) and (110) show in-plane magnetic anisotropies reflecting the magnetocrystalline anisotropies of bulk Fe-Si alloy crystals. The Fe-Si films deposited on MgO(111) show nearly isotropic in-plane magnetic anisotropies that possibly come from the multiple variant structure. The coercivity decreases with increasing the Si composition and with decreasing the substrate temperature.

Keywords: $Fe_{100-x}Si_x$ (x = 0 − 10 at. %) alloy, epitaxial thin film, MgO single-crystal substrate, soft magnetic property

1. Introduction

Fe-Si alloy is a typical soft magnetic material and has been used in transformers, motors, etc. It is known that the crystallographic structure and the magnetic properties change depending on the Si composition and the processing temperature[1,2]. In particular, Fe − 3 wt. % Si (≈ Fe − 6 at. % Si) alloys are widely used in the related industries because of excellent soft magnetic properties with high permeability, high saturation magnetization (M_s), and low coercivity (H_c). In such applications, grain-oriented or non-grain-oriented silicon steel sheets are generally employed, where the overall magnetic properties are influenced by the structure consisting of crystal grains. Therefore, understanding the magnetic properties of Fe-Si crystals with different orientations is very important to further improve the overall soft magnetic properties.

There are some reports on the investigations concerning the relationships of Si/Fe composition and crystallographic orientation with respect to the magnetic properties by using bulk Fe-Si single-crystal materials[3,4]. However, it is not easy to prepare bulk crystal samples systematically varying the Si composition or the crystallographic orientation. In contrast, it seems possible to prepare thin film crystal samples, where the composition and the crystallographic orientation can be respectively controlled by the target composition and the orientation of single-crystal substrate. In the present study,

$Fe_{100-x}Si_x$ (at. %, x = 0 − 10) alloy thin films are prepared on MgO single-crystal substrates of (001), (110). and (111) orientations at temperatures ranging from room temperature (RT) to 600 °C. The influences of film composition, substrate temperature, and substrate orientation on the detailed structure and the magnetic properties are systematically investigated.

2. Experimental Procedure

$Fe_{100-x}Si_x$ (x = 0, 2, 6, 10 at. %) alloy films of 40 nm thickness were deposited on polished MgO substrates of (001), (110), and (111) orientations by using a radio-frequency (RF) magnetron sputtering system equipped with a reflection high-energy electron diffraction (RHEED) facility. The base pressures were lower than 4×10^{-7} Pa. Before film formation, substrates were heated at 600 °C for 1 hour to obtain clean surfaces. The distance between a target and substrates was fixed at 150 mm. The Ar gas pressure was kept constant at 0.67 Pa. The RF powers for Fe, $Fe_{98}Si_2$, $Fe_{94}Si_6$, and $Fe_{90}Si_{10}$ targets were respectively fixed at 52, 59, 54, and 54 W, where the deposition rates were 0.02 nm/s. The substrate temperature was varied in a range from RT to 600 °C.

The surface structure was studied by RHEED. The resulting film structure was investigated by $2\theta/\omega$ scan out-of-plane and $2\theta\chi/\varphi$ scan in-plane X-ray diffractions (XRDs) with Cu-Kα radiation (λ = 0.15418 nm). The surface morphology was observed by atomic force
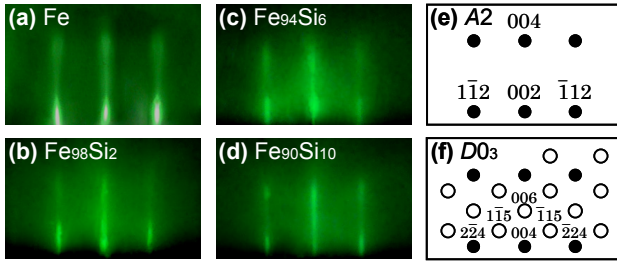
Fig. 1 RHEED patterns observed for (a) Fe, (b) $Fe_{98}Si_2$, (c) $Fe_{94}Si_6$, and (d) $Fe_{90}Si_{10}$ films prepared on MgO(001) substrates at 200 °C. [(e), (f)] Schematic diagrams of RHEED patterns of (e) $A2$(001) and (f) $D0_3$(001) single-crystal surfaces simulated by using the lattice constants of bulk (e) Fe (a = 0.2866 nm[6]) and (f) Fe_3Si (a = 0.5653 nm[7]), respectively. The incident electron beam is parallel to (a)–(d) MgO[100], (e) $A2$[110], or (f) $D0_3$[110]. The filled and open circles in (f) respectively correspond to the fundamental and the superlattice reflections.

microscopy (AFM). The magnetization curves were measured by vibrating sample magnetometry.

3. Results and Discussion

3.1 Effect of Si/Fe composition

Figures 1(a)–(d) show the RHEED patterns observed for $Fe_{100-x}Si_x$ alloy films with x = 0 – 10 at. % deposited on MgO(001) substrates at 200 °C. Clear diffraction patterns are observed for all the investigated compositions. The Fe-Si films grow epitaxially on the substrates. bcc-based disordered $A2$ phase and ordered $D0_3$ phase exist in Fe-rich region of the bulk Fe-Si binary alloy phase diagram[5]. Diffraction patterns for $A2$(001) and $D0_3$(001) surfaces were thus calculated by using the lattice constants of bulk Fe (a = 0.2866 nm[6]) and Fe_3Si (a = 0.5653 nm[7]), respectively. Figures 1(e) and (f) are the schematic diagrams of the simulated patterns of $A2$(001) and $D0_3$(001) surfaces, respectively. The observed RHEED patterns are corresponding to the pattern simulated for $A2$(001) surface. The epitaxial orientation relationship is determined as

$A2$(001)[110] ∥ MgO(001)[100].

Fe-Si(001) single-crystal films with $A2$ structure are obtained on the substrates, where the Fe-Si(001) lattice is rotated around the film normal by 45° with respect to the MgO(001) lattice. In this configuration, the lattice mismatch slightly increases from −4.0% to −4.4% with increasing the x value from 0 to 10 at. %, where the lattice constants of bulk MgO (a = 0.4217 nm[8]), Fe (a = 0.2866 nm[6]), and $Fe_{89.5}Si_{10.5}$ (a = 0.2853 nm[9]) crystals are used.

Figures 2(a-1)–(d-1) and 3(a-1)–(d-1) show the out-of-plane and in-plane XRD patterns measured for Fe-Si films. Here, the scattering vector of in-plane XRD is parallel to MgO[1$\bar{1}$0]. Out-of-plane $A2$(002) and in-plane $A2$(200) fundamental reflections are recognized, whereas out-of-plane $D0_3$(002) and in-plane $D0_3$(200)
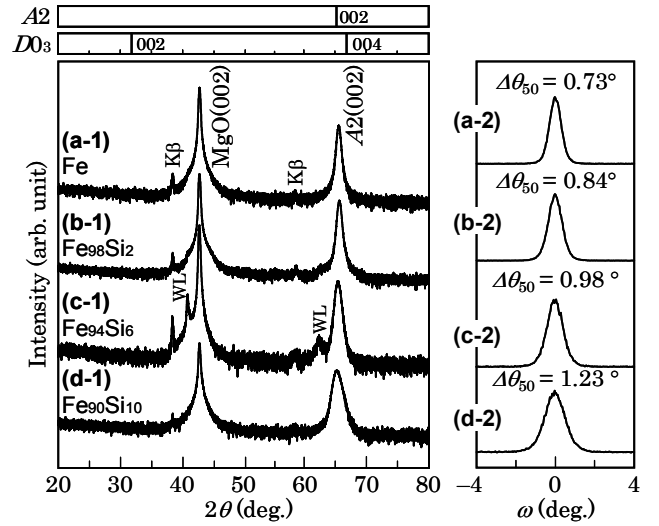
Fig. 2 (a-1)–(d-1) Out-of-plane XRD patterns measured for (a) Fe, (b) $Fe_{98}Si_2$, (c) $Fe_{94}Si_6$, and (d) $Fe_{90}Si_{10}$ films prepared on MgO(001) substrates at 200 °C. (a-2)–(d-2) Rocking curves measured by fixing the diffraction angle of 2θ at the peak angles of $A2$(002) reflections in the patterns of (a-1)–(d-1), respectively. The intensity is shown in (a-1)–(d-1) logarithmic or (a-2)–(d-2) linear scale.
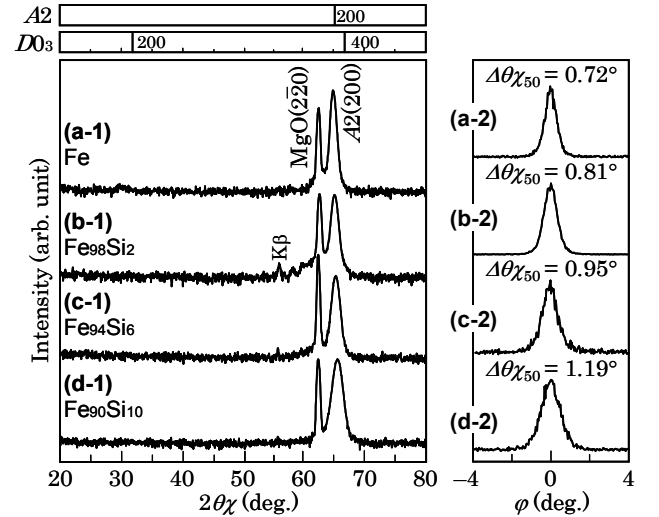
Fig. 3 (a-1)–(d-1) In-plane XRD patterns measured for (a) Fe, (b) $Fe_{98}Si_2$, (c) $Fe_{94}Si_6$, and (d) $Fe_{90}Si_{10}$ films prepared on MgO(001) substrates at 200 °C. The scattering vector is parallel to MgO[110]. (a-2)–(d-2) Rocking curves measured by fixing the diffraction angle of $2\theta\chi$ at the peak angles of $A2$(200) reflections in the patterns of (a-1)–(d-1), respectively. The intensity is shown in (a-1)–(d-1) logarithmic or (a-2)–(d-2) linear scale.

superlattice reflections are absent. The XRD confirms the crystal structure and the epitaxial orientation relationship determined by RHEED.

Figure 4(a) shows the Si composition dependences of lattice constants, a and c, of Fe-Si film. The lattice constants are calculated by using the relation of (a, c) = $(2d_{A2(200)}, 2d_{A2(002)})$. The Fe-Si lattices are slightly
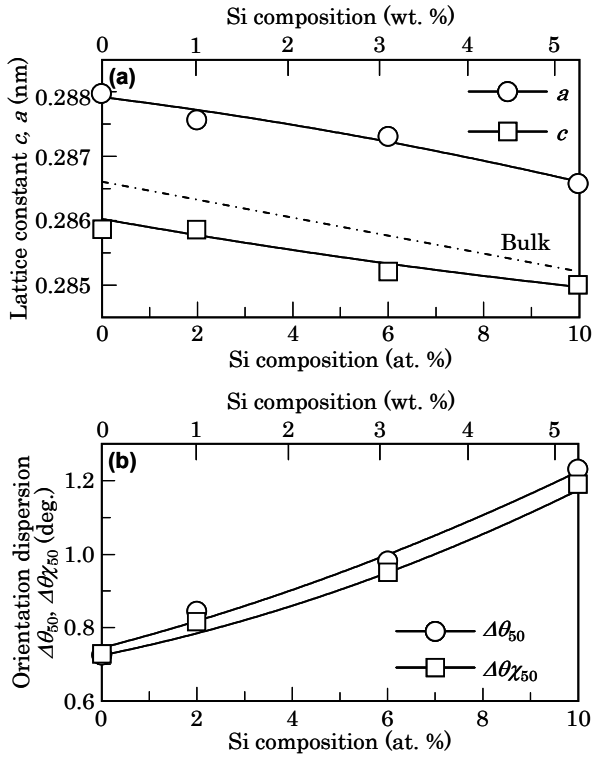
Fig. 4 Compositional dependences of (a) lattice constants of a and c and (b) orientation dispersion values of $\Delta\theta_{50}$ and $\Delta\theta\chi_{50}$ of Fe-Si film prepared on MgO(001) substrate at 200 °C. The lattice constants of bulk Fe-Si crystals are cited from Ref. 9.

deformed along the c-axis due to accommodation of lattice misfits of about −4%. With increasing the Si composition, a and c values are decreasing. The out-of-plane and in-plane orientation dispersions ($\Delta\theta_{50}$, $\Delta\theta\chi_{50}$) are respectively estimated as the full widths at half maximum of rocking curves measured by fixing the diffraction angles of 2θ and $2\theta\chi$ at the peak angles of out-of-plane $A2(002)$ and in-plane $A2(200)$ reflections, as shown in Figs. 2(a-2)–(d-2) and 3(a-2)–(d-2). Figure 4(b) shows the Si composition dependences of $\Delta\theta_{50}$ and $\Delta\theta\chi_{50}$. With increasing the Si composition, $\Delta\theta_{50}$ and $\Delta\theta\chi_{50}$ values are increasing. These results indicate that Si composition in Fe-Si film affects delicately the crystal unit cell size and the crystallographic quality.

Figure 5 shows the magnetization curves, where the rotation angle of θ_H shows the applied field direction with respect to $A2[100]$ in $A2(001)$. These films are easily magnetized when the magnetic field is applied along $A2[100]$, while the magnetization curves measured along $A2[110]$ saturate at higher fields. Therefore, the magnetic properties of these films are reflecting the magnetocrystalline anisotropy of bulk Fe-Si crystal with $A2$ structure.

It is recognized that the magnetization curve measured along $A2[110]$ saturates at a lower magnetic field and the coercivity decreases with increasing the Si composition from 0 to 10 at. %. The magnetic property will be explained by considering magnetocrystalline
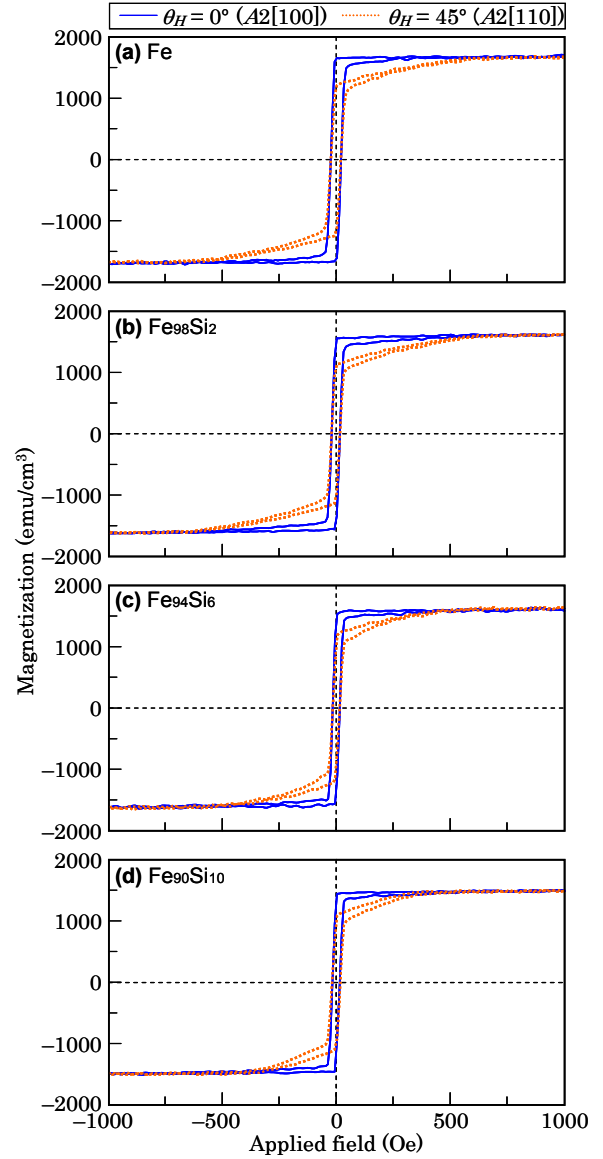
Fig. 5 Magnetization curves measured for (a) Fe, (b) Fe98Si2, (c) Fe94Si6, and (d) Fe90Si10 films prepared on MgO(001) substrates at 200 °C.
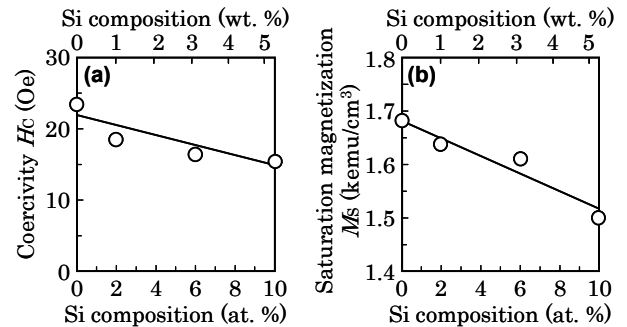
Fig. 6 Compositional dependences of (a) H_c and (b) M_s values of Fe-Si films prepared on MgO(001) substrate at 200 °C.

anisotropy energy. When the magnetization rotates in $A2(001)$, the magnetic free energy is expressed as
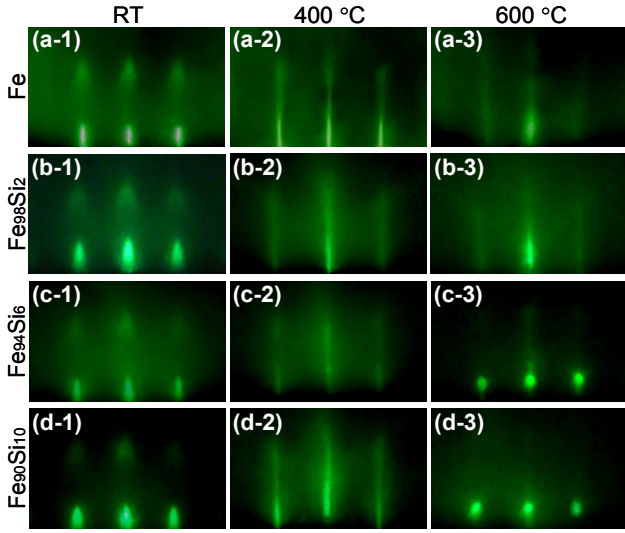
Fig. 7 RHEED patterns observed for (a) Fe, (b) $Fe_{98}Si_2$, (c) $Fe_{94}Si_6$, and (d) $Fe_{90}Si_{10}$ films prepared on MgO(001) substrates at (a-1)–(d-1) RT, (a-2)–(d-2) 400 °C, and (a-3)–(d-3) 600 °C. The incident electron beam is parallel to MgO[100].

$$E_a = \frac{1}{8} \cdot K_1 \cdot (1 - \cos 4\theta_M), \qquad (1)$$

where K_1 is the magnetic anisotropy energy and θ_M is the direction of magnetization. For Fe and Fe-Si alloy, K_1 is positive. Then, E_a becomes minimum at $\theta_M = 0°$, 90° and becomes maximum at $\theta_M = 45°$. Therefore, $A2[100]$ is the easy magnetization axis and $A2[110]$ is the hard magnetization axis. This calculation is well explaining the measured magnetization curves. Figure 6 shows the Si composition dependences of coercivity (H_c) and saturation magnetization (M_s). Here, M_s value is regarded as the magnetization of Fe-Si film measured at 5 kOe. With increasing the Si composition from 0 to 10 at. %, the M_s value decreases linearly by about 11 %, and the H_c value decreases from 24 to 16 Oe reflecting the soft magnetic property of Fe-Si alloy.

3.2 Effect of substrate temperature

Figure 7 shows the RHEED patterns observed for Fe-Si films with different Si compositions grown on MgO(001) substrates at RT, 400, and 600 °C. Clear diffraction patterns corresponding to $A2(001)$ surface are recognized for all the compositions, whereas any patterns corresponding to $D0_3(001)$ surface are not recognized.

Figure 8 shows the substrate temperature dependences on lattice constants, a, and c, of Fe-Si films with different Si compositions. With increasing the substrate temperature, c value increases, while a value decreases for all the Si compositions.

Figure 9 shows the substrate temperature dependences on out-of-plane and in-plane orientation dispersions, $\Delta\theta_{50}$ and $\Delta\theta\chi_{50}$. With increasing the substrate temperature, the $\Delta\theta_{50}$ and $\Delta\theta\chi_{50}$ values decreases for all the Si compositions. The
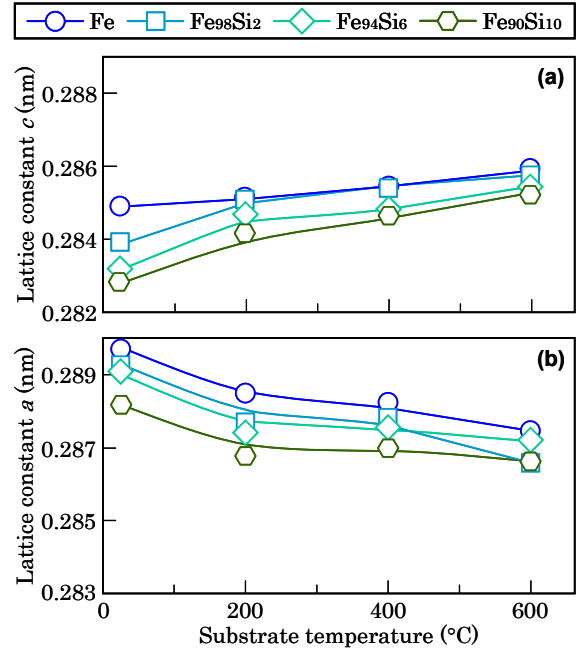
Fig. 8 Substrate temperature dependences of (a) c and (b) a values of Fe, $Fe_{98}Si_2$, $Fe_{94}Si_6$, and $Fe_{90}Si_{10}$ films prepared on MgO(001) substrates.
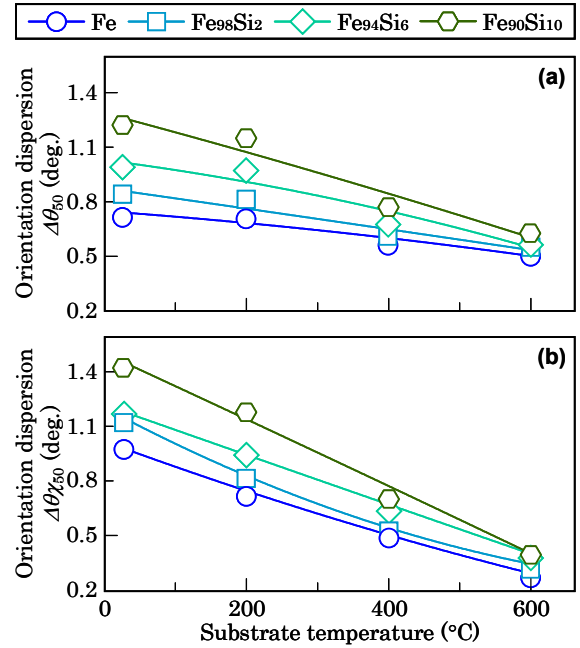
Fig. 9 Substrate temperature dependences of (a) $\Delta\theta_{50}$ and (b) $\Delta\theta\chi_{50}$ of Fe, $Fe_{98}Si_2$, $Fe_{94}Si_6$, and $Fe_{90}Si_{10}$ films prepared on MgO(001) substrates.

crystallographic quality of Fe-Si film is improving possibly through relaxation of film stress caused by lattice mismatch with the substrate.

Figure 10 shows the AFM images observed for Fe-Si films with different Si compositions deposited at different temperatures. The films deposited at RT, 200, and 400 °C have flat surfaces with the arithmetical mean roughness (R_a) values less than 2 nm. On the
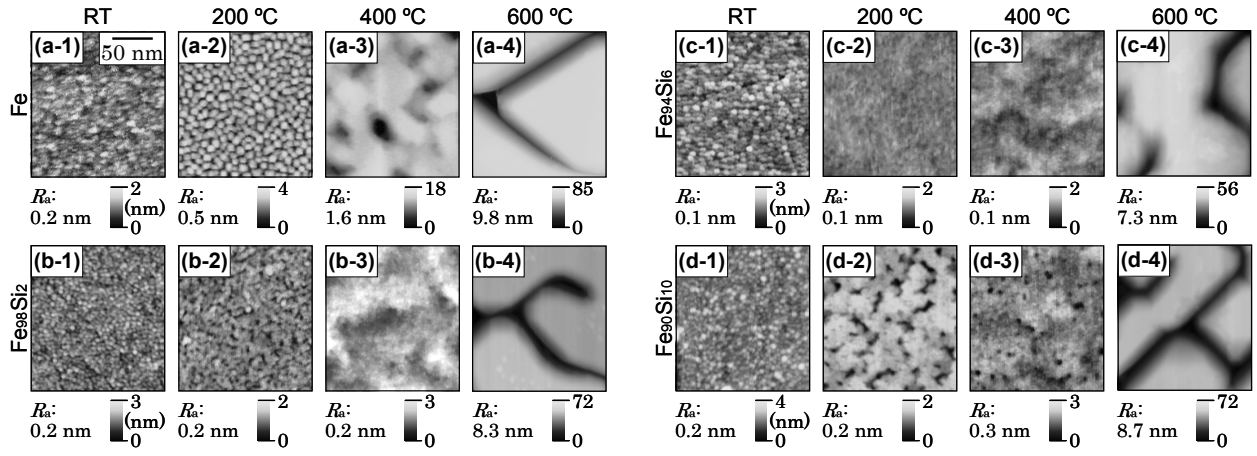
Fig. 10 AFM images observed for (a) Fe, (b) $Fe_{98}Si_2$, (c) $Fe_{94}Si_6$, and (d) $Fe_{90}Si_{10}$ films prepared on MgO(001) substrates at (a-1)–(d-1) RT, (a-2)–(d-2) 200 °C, (a-3)–(d-3) 400 °C, and (a-4)–(d-4) 600 °C.
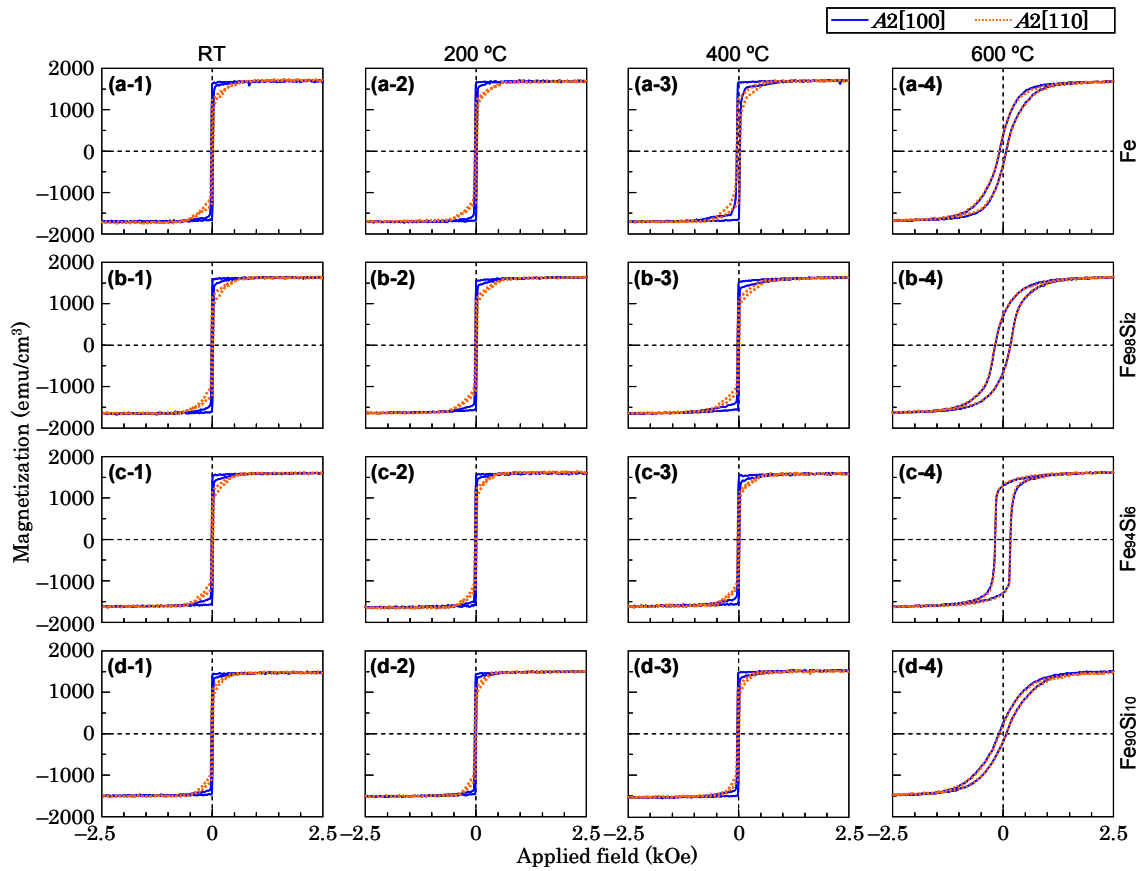
Fig. 11 Magnetization curves measured for (a) Fe, (b) $Fe_{98}Si_2$, (c) $Fe_{94}Si_6$, and (d) $Fe_{90}Si_{10}$ films prepared on MgO(001) substrates at (a-1)–(d-1) RT, (a-2)–(d-2) 200 °C, (a-3)–(d-3) 400 °C, and (a-4)–(d-4) 600 °C.

contrary, the R_a values of films deposited at 600 °C are greater than 7 nm, where large islands with faceted faces are formed as shown in Figs. 10(a-4)–(d-4). It is considered that migrations of deposited atoms are enhanced at a higher substrate temperature. The variation of surface roughness as a function of substrate temperature is similar in these Fe-Si films.

Figure 11 shows the magnetization curves of Fe-Si films at different substrate temperatures. The films deposited at RT, 200, and 400 °C show the magnetic properties reflecting the magnetocrystalline anisotropy of bulk Fe-Si crystal with $A2$ structure. With increasing the substrate temperature up to 600 °C, the difference in the curves measured along $A2$[110] and $A2$[100] becomes small. The films are almost magnetically isotropic in in-plane measurements. The reason is possibly due to the shape anisotropy caused by the surface undulation as shown in Figs. 10(a-4)–(d-4).
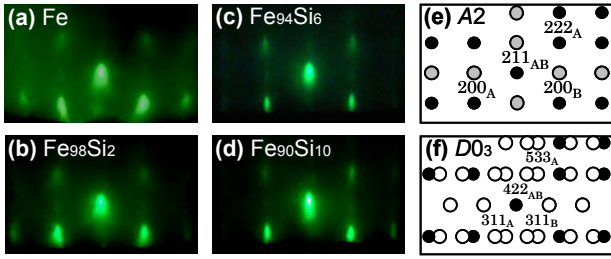
Fig. 12 RHEED patterns observed for (a) Fe, (b) $Fe_{98}Si_2$, (c) $Fe_{94}Si_6$, and (d) $Fe_{90}Si_{10}$ films prepared on MgO(110) substrates at 200 °C. [(e), (f)] Schematic diagrams of RHEED patterns of (e) $A2$(211) and (f) $D0_3$(211) single-crystal surfaces simulated by using the lattice constants of bulk (e) Fe and (f) Fe_3Si, respectively. The incident electron beam is parallel to (a)–(d) MgO[001]. The filled and open circles in (f) respectively correspond to the fundamental and the superlattice reflections. The reflections indicated by the gray circles in (e) show that the $A2$(211) plane has a reconstructed surface of $p(3\times1)$.
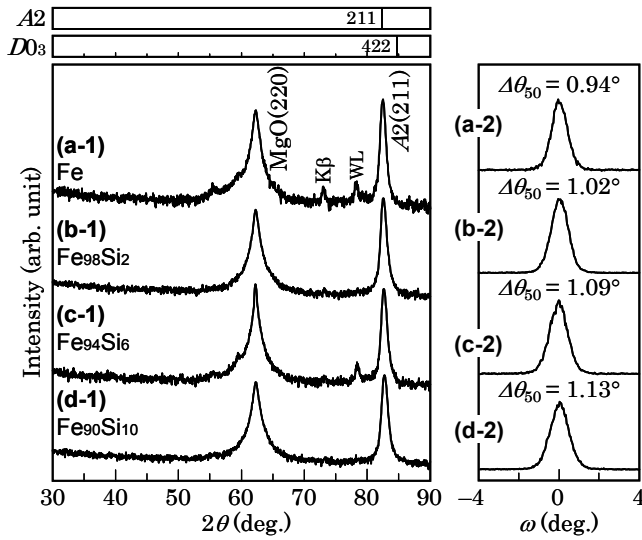
Fig. 13 (a-1)–(d-1) Out-of-plane XRD patterns measured for (a) Fe, (b) $Fe_{98}Si_2$, (c) $Fe_{94}Si_6$, and (d) $Fe_{90}Si_{10}$ films prepared on MgO(110) substrates at 200 °C. (a-2)–(d-2) Rocking curves measured by fixing the diffraction angle of 2θ at the peak angles of $A2$(211) reflections in the patterns of (a-1)–(d-1), respectively. The intensity is shown in (a-1)–(d-1) logarithmic or (a-2)–(d-2) linear scale.

3.3 Effect of substrate orientation

Figures 12(a)–(d) show the RHEED patterns observed for Fe-Si films with different Si compositions deposited on MgO(110) substrates at 200 °C. Clear diffraction patterns corresponding to $A2$(211) surface are recognized, whereas diffractions corresponding to $D0_3$(211) surface are not observed, where the schematic diagrams of RHEED patterns from $A2$(211) and $D0_3$ (211) are respectively shown in Figs. 12(e) and (f). The $A2$(211) RHEED pattern consists of two reflections, as shown by the spots A and B in the diagram of Fig. 12(e).
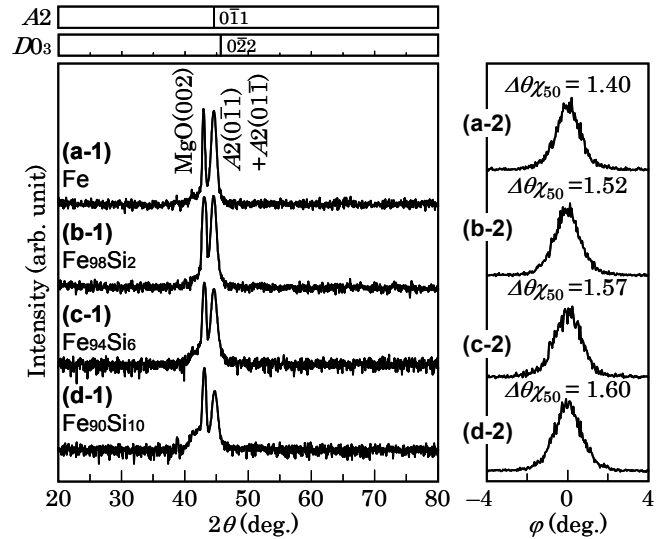
Fig. 14 (a-1)–(d-1) In-plane XRD patterns measured for (a) Fe, (b) $Fe_{98}Si_2$, (c) $Fe_{94}Si_6$, and (d) $Fe_{90}Si_{10}$ films prepared on MgO(110) substrates at 200 °C. The scattering vector is parallel to MgO[001]. (a-2)–(d-2) Rocking curves measured by fixing the diffraction angle of $2\theta\chi$ at the peak angles of $A2(0\bar{1}1) + A2(01\bar{1})$ reflections in the patterns of (a-1)–(d-1), respectively. The intensity is shown in (a-1)–(d-1) logarithmic or (a-2)–(d-2) linear scale.
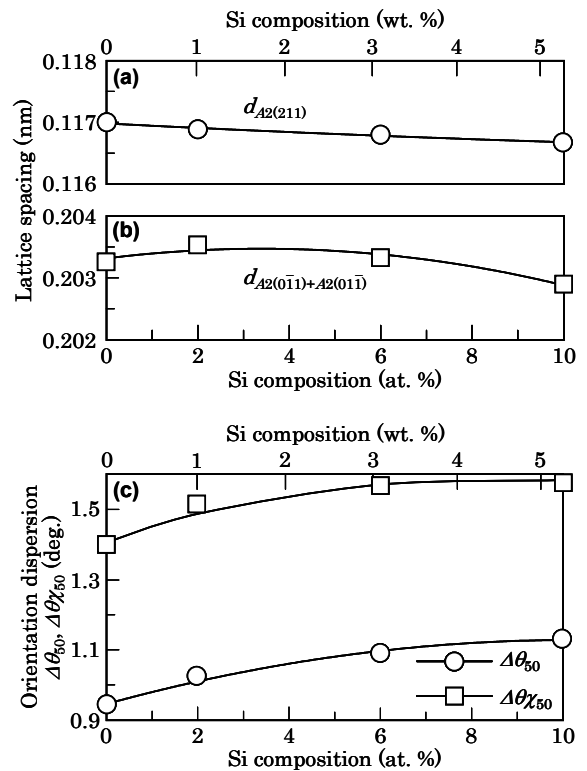
Fig. 15 Compositional dependences of (a) $d_{A2(211)}$, (b) $d_{A2(0\bar{1}1)+A2(01\bar{1})}$, and (c) $\Delta\theta_{50}$ and $\Delta\theta\chi_{50}$ of Fe-Si film prepared on MgO(110) substrate at 200 °C.

The epitaxial orientation relationship is determined from the RHEED observation as follows,

$A2(211)[0\bar{1}1] \parallel \text{MgO}(110)[001],$ (type A)

$A2(211)[01\bar{1}] \parallel \text{MgO}(110)[001].$ (type B)

The Fe-Si(211) films consist of two types of variant whose orientations are rotated around the film normal by 180° each other. In this configuration, the lattice misfit value differs depending on the in-plane direction at the Fe-Si/MgO interface. The lattice misfit value along MgO[001] is about −4%. Although there exists a fairly large mismatch of around −17% along MgO[110], epitaxial growth of Fe-Si crystal is taking place. This type of epitaxial growth where misfit dislocations are introduced at the interface is reported for the Cr/MgO system[10,11]. The mismatch is considered to be reduced through introduction of misfit dislocations in the film around the Fe-Si/MgO interface.
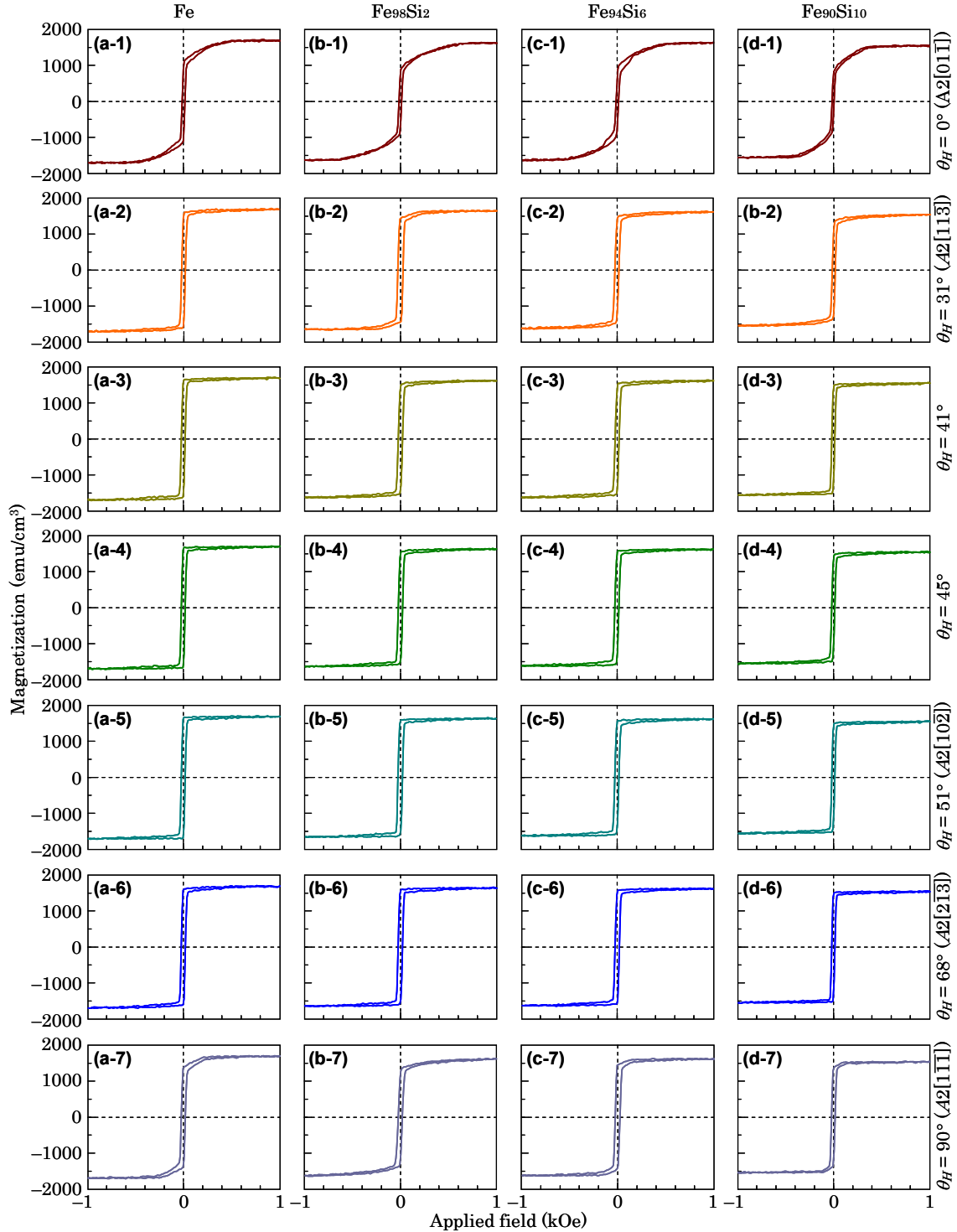
Fig. 16 Magnetization curves measured for (a) Fe, (b) Fe$_{98}$Si$_2$, (c) Fe$_{94}$Si$_6$, and (d) Fe$_{90}$Si$_{10}$ films prepared on MgO(110) substrates at 200 °C.

Figures 13(a-1)–(d-1) show the out-of-plane XRD patterns of Fe-Si films deposited on MgO(110) substrates. $A2(211)$ reflections are recognized, whereas $D0_3(211)$ reflections are not recognized. Figures 14(a-1)–(d-1) show the in-plane XRD patterns. Only the reflections from $A2$ crystals and the MgO substrates are recognized for these films. Figure 15 shows the Si composition dependences of lattice spacing, $d_{A2(211)}$ and $d_{A2(0\bar{1}1)+A2(01\bar{1})}$, and orientation dispersion of $\Delta\theta_{50}$ and $\Delta\theta\chi_{50}$ of these films. With increasing the Si composition, the $d_{A2(211)}$ and $d_{A2(0\bar{1}1)+A2(01\bar{1})}$ values are slightly decreasing, whereas the $\Delta\theta_{50}$ and $\Delta\theta\chi_{50}$ values are increasing similar to the case of Fe-Si/MgO(001) system.

Figures 16(a)–(d) show the magnetization curves of Fe-Si films deposited on MgO(110) substrates. Here, θ_H is the direction of magnetic field applied to the sample expressed in angle measured from $A2[01\bar{1}]$ direction in the $A2(211)$ film plane. These films are easily magnetized when the magnetic field is applied along around $\theta_H = 45°$, while the magnetization curves measured along $\theta_H = 0°$ and $90°$ saturate at higher fields. Figure 17 shows the pole-figure maps indicating the distribution of low-index planes including $A2\{100\}$ planes. The angle of $A2[01\bar{1}]$ and in-plane component of $A2(010)$ is $41°$. The magnetic free energy is written in the following equation when the magnetization rotates in (211) plane,

$$E_a = \frac{1}{12} \cdot K_1 \cdot (4 - 8\cos^2\theta_M + 7\cos^4\theta_M). \tag{2}$$

Figure 18 shows the anisotropy energy, E_a, as a function of θ_M calculated by using the equation (2). It is shown that the easy magnetization axis lies along $\theta_M = 41°$ or $139°$ and the first hard magnetization axis lies along $A2[1\bar{1}\bar{1}]$ and the second hard magnetization axis lies along $A2[01\bar{1}]$. When the measured magnetization curves shown in Figs. 16 are compared with the calculation, it is noted that the angle-direction of easy magnetization axis is in agreement with the calculation for all the compositions. However, the experimental data shown in Fig. 16 show that the first hard magnetization axis lies parallel to $A2[01\bar{1}]$ and the second one lies parallel to $A2[1\bar{1}\bar{1}]$. There is a difference in the order of magnetization hardness, suggesting that there exists an additional influence from the film detailed structure. The XRD data shown in Fig. 15(c) indicate that the dispersion in Fe-Si film sample varies depending on the crystallographic orientation which suggests the presence of anisotropic film distortion. Such kind of distortion may have affected the magnetocrystalline anisotropy.

Figure 19 shows the Si composition dependences of H_c and M_s values of Fe-Si film deposited on MgO(110) substrate. With increasing the Si composition from 0 to 10 at. %, the M_s value decreases linearly by about 13 %, and the H_c value decreases from 28 to 19 Oe reflecting the soft magnetic property of Fe-Si alloy.

Figures 20(a)–(d) show the RHEED patterns
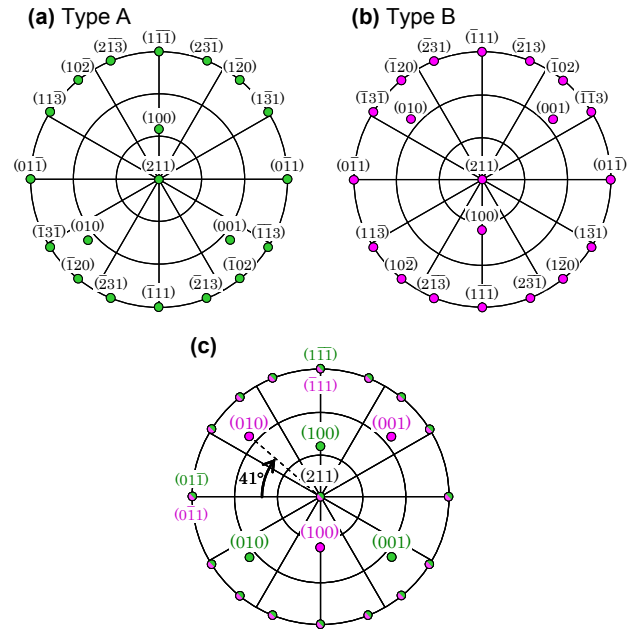
Fig. 17 Pole-figure maps showing the configurations of $A2\{100\}$ planes of (a) type A, (b) type B, and (c) type A + B, where $A2(211)$ is centered.
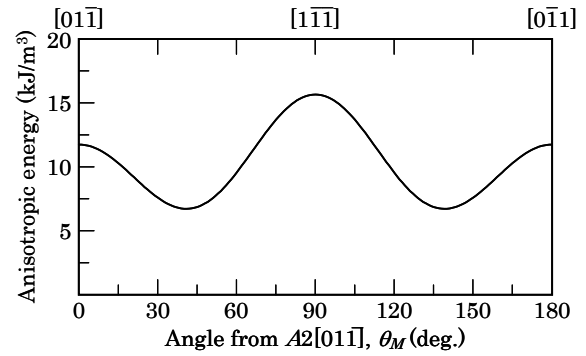
Fig. 18 Anisotropy energy in $A2(211)$ as a function of magnetization direction. K_1 is set to 47 kJ/m^3.
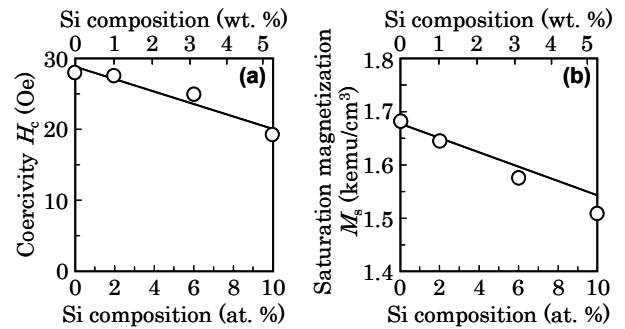
Fig. 19 Compositional dependences on (a) H_c and (b) M_s values of Fe-Si films prepared on MgO(110) substrates at 200 °C.

observed for Fe-Si films deposited on MgO(111) substrates at 200 °C. Clear RHEED patterns corresponding to $A2(110)$ texture [Fig. 20(e)] are observed. These RHEED patterns consist of two
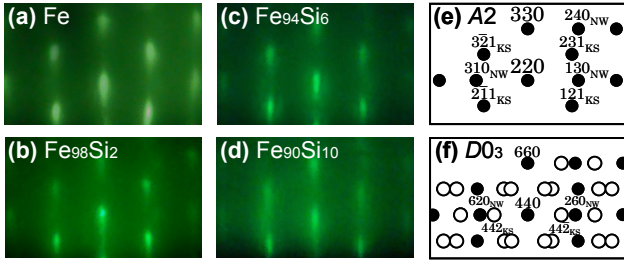
Fig. 20 RHEED patterns observed for (a) Fe, (b) Fe$_{98}$Si$_2$, (c) Fe$_{94}$Si$_6$, and (d) Fe$_{90}$Si$_{10}$ films prepared on MgO(111) substrates at 200 °C. [(e), (f)] Schematic diagrams of RHEED patterns of (e) $A2$(110) and (f) $D0_3$(110) single-crystal surfaces simulated by using the lattice constants of bulk (e) Fe and (f) Fe$_3$Si, respectively. The incident electron beam is parallel to (a)–(d) MgO[1$\bar{1}$0], (e) $A2$[001] and $A2$[$\bar{1}$10], or (f) $D0_3$[001] and $D0_3$[110]. The filled and open circles in (f) respectively correspond to the fundamental and the superlattice reflections.
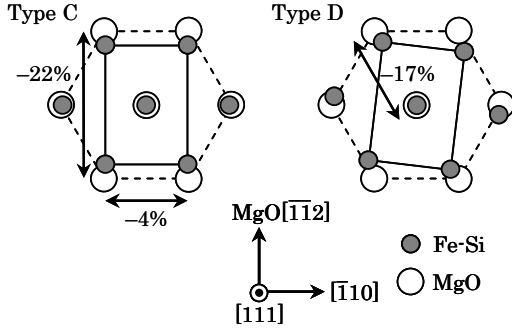
Fig. 21 Epitaxial orientation relationships of Fe-Si(110) ∥ MgO(111).

reflections, as shown by the spots C and D in the spot map of Fig 20(e). The epitaxial orientation relationship is determined by RHEED as follows,

$A2$(110)[001] ∥ MgO(111)[1$\bar{1}$0],　　　　　　(type C)

$A2$(110)[11$\bar{1}$] ∥ MgO(111)[1$\bar{1}$0].　　　　　(type D)

When the atomic arrangement of MgO(111) surface which shows six-fold symmetry with respect to the perpendicular direction is considered, the $A2$(110) crystals of types C and D are interpreted to be consisting of three and six variants whose orientations are rotated around the film normal by 120° and 60° each other, respectively. The crystallographic orientation relationships of types C and D are similar to the Nishiyama-Wasserman (NW)[12,13] and the Kurdjumov-Sachs (KS)[14] relationships, respectively. In these configurations, as shown in Fig. 21, large lattice mismatches along MgO[11$\bar{2}$], –22%, and MgO[1$\bar{1}$0], –17%, are involved at the $A2$(110)$_{\text{type C}}$/MgO(111) and the $A2$(110)$_{\text{type D}}$/MgO(111) interfaces. The crystallographic orientation relationships observed in the present study is similar to those reported for the Fe-based alloy films with bcc(110) orientation formed on MgO(111) substrates[15,16].
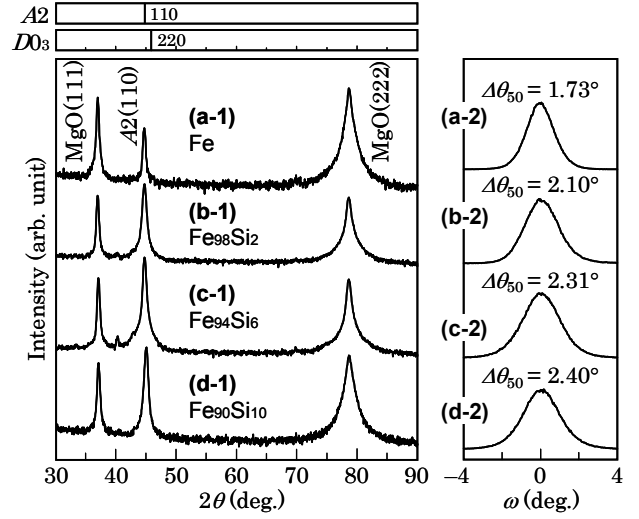
Fig. 22 (a-1)–(d-1) Out-of-plane XRD patterns measured for (a) Fe, (b) Fe$_{98}$Si$_2$, (c) Fe$_{94}$Si$_6$, and (d) Fe$_{90}$Si$_{10}$ films prepared on MgO(111) substrates at 200 °C. (a-2)–(d-2) Rocking curves measured by fixing the diffraction angle of 2θ at the peak angles of $A2$(110) reflections in the patterns of (a-1)–(d-1), respectively. The intensity is shown in (a-1)–(d-1) logarithmic or (a-2)–(d-2) linear scale.
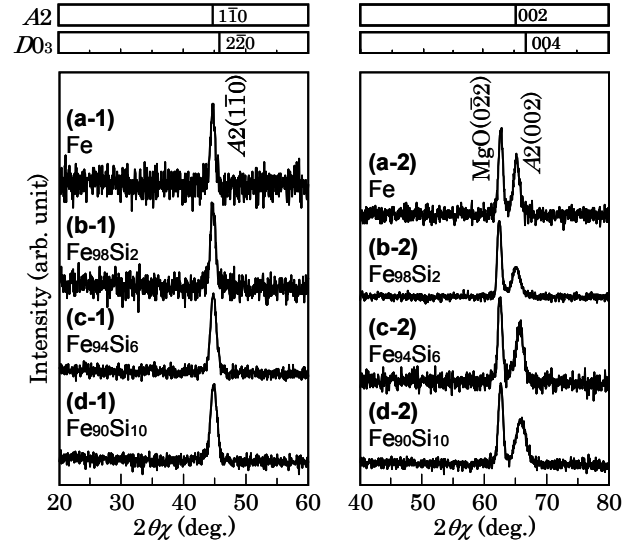
Fig. 23 (a)–(d) In-plane XRD patterns measured for (a) Fe, (b) Fe$_{98}$Si$_2$, (c) Fe$_{94}$Si$_6$, and (d) Fe$_{90}$Si$_{10}$ films prepared on MgO(111) substrates at 200 °C. The scattering vector is parallel to (a-1)–(d-1) MgO[11$\bar{2}$] or (a-2)–(d-2) MgO[1$\bar{1}$0]. The intensity is shown in logarithmic scale.

Figures 22(a-1)–(d-1) and 23(a-1)–(d-2) show the out-of-plane and in-plane XRD patterns of Fe-Si films deposited on MgO(111) substrates, respectively. Reflections from $A2$ crystals are recognized, whereas Reflections from $D0_3$ are not recognized.

Figure 24 shows the Si composition dependences of lattice constants, $\Delta\theta_{50}$, and $\Delta\theta\chi_{50}$. The lattice constants are calculated by using the relation of
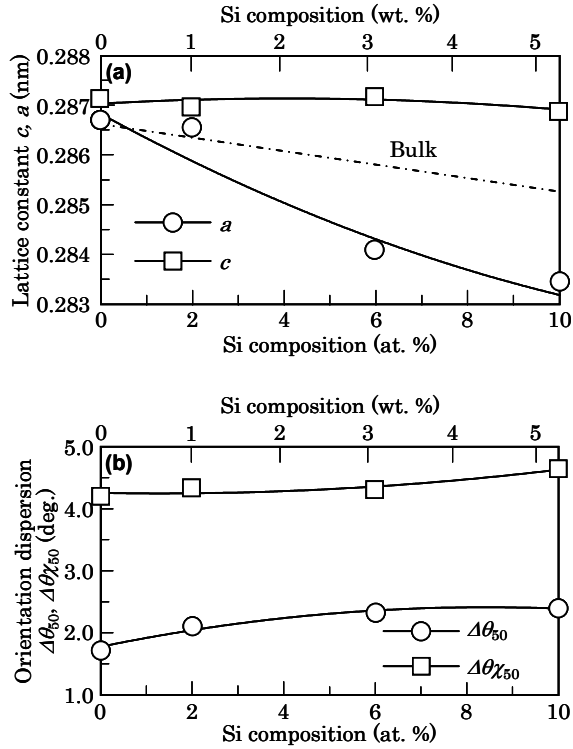
Fig. 24 Compositional dependences of (a) a and c and (b) $\Delta\theta_{50}$ and $\Delta\theta\chi_{50}$ of Fe-Si films prepared on MgO(111) substrate at 200 °C.

$$a = (d_{A2(110)}{}^2 + d_{A2(1\bar{1}0)}{}^2)^{1/2}, \qquad (3)$$

$$c = 2d_{A2(002)}. \qquad (4)$$

The Fe-Si lattices are slightly deformed along the c-axis in accommodation of lattice misfits of about −4%. With increasing the Si composition, the a value is decreasing, while the c value does not change much. The $\Delta\theta_{50}$ and $\Delta\theta\chi_{50}$ values are increasing with increasing the Si composition.

Figure 25 shows the magnetization curves. Here, θ_H is the direction of magnetic field applied to the sample expressed in angle measured from $A2[001]$ direction in the $A2(110)$ film plane. The magnetic free energy is written in the following equation when the magnetization rotates in (110) plane,

$$E_a = \frac{1}{32} \cdot K_1 \cdot (7 - 4\cos 2\theta_M - 3\cos 4\theta_M). \qquad (4)$$

Figure 26 shows the anisotropy energy, E_a, as a function of θ_M calculated by using the equation (4). It is shown that the easy magnetization axis lies along $A2[001]$. Indeed, it was reported that Fe(110) single-crystal films were easily magnetized when the magnetic field was applied along the Fe[001] direction[17]. However, the films prepared in the present study show nearly isotropic in-plane magnetic anisotropies. This is possibly because that the films prepared in the present study are not single-crystals but epitaxial thin films consisting of three and six variants whose orientations are rotated around the film normal by 120° and 60° each other (Fig. 21). In this
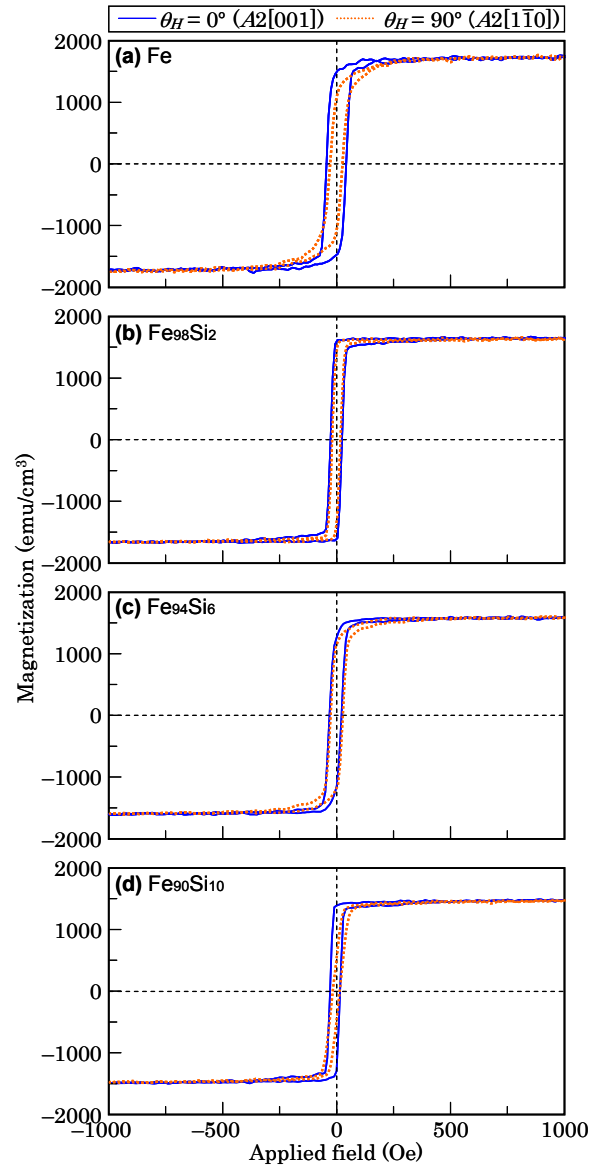
Fig. 25 Magnetization curves measured for (a) Fe, (b) Fe$_{98}$Si$_2$, (c) Fe$_{94}$Si$_6$, and (d) Fe$_{90}$Si$_{10}$ films grown on MgO(111) substrates at 200 °C.
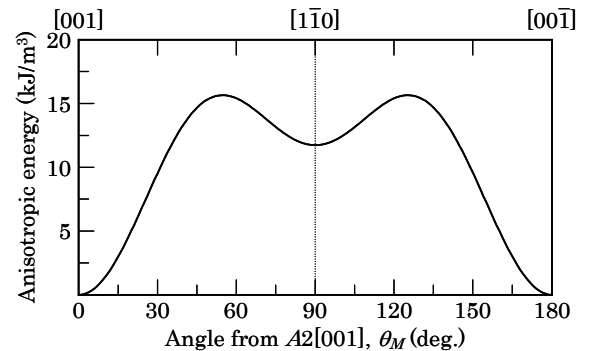
Fig. 26 Anisotropy energy in $A2(110)$ as a function of magnetization direction. K_1 is set to 47 kJ/m^3.

case, the in-plane magnetic property of epitaxial thin film will be influenced by the distribution of variant
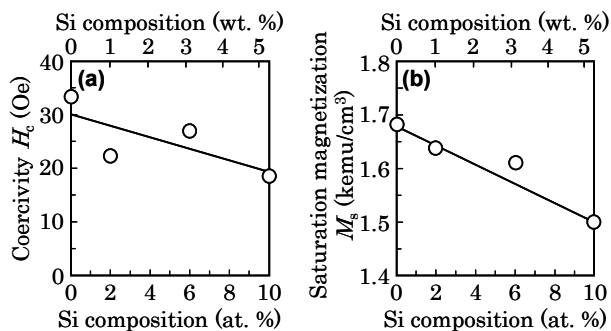
Fig. 27 Compositional dependences on (a) H_c and (b) M_s values of Fe-Si films prepared on MgO(111) substrates at 200 °C.

crystals. The almost isotropic in-plane magnetic anisotropies observed for the epitaxial thin films are due to the complex variant structure.

Figure 27 shows the compositional dependences of H_c and M_s values. With increasing the Si composition from 0 to 10 at. %, the M_s value decreases linearly by about 12 %, and the H_c value decreases from 34 to 19 Oe reflecting the soft magnetic property of Fe-Si alloy.

In the present study, $Fe_{100-x}Si_x$ ($x = 0 - 10$ at. %) epitaxial films are prepared on MgO single-crystal substrates under similar experimental conditions. It is shown that single-crystal films of (001) orientation grow on MgO(001), bi-crystalline epitaxial films with (211) orientation grow on MgO(110), and epitaxial films consisting of two types of (110) variant grow on MgO(111) substrates. Although they are epitaxial thin film crystals, differences in quality and magnetic properties are noted between these samples. For example when the $\Delta\theta_{50}$ value, out-of-plane dispersion which is a measure of crystallographic quality, is compared between the samples prepared at 200 °C, lower values are observed in the order of samples prepared on MgO(001) < MgO(110) < MgO(111) for the investigated compositional range. The $\Delta\theta_{50}$ value is increasing with increasing the Si composition for all cases. Similar tendency is also noted in the variation of $\Delta\theta\chi_{50}$, in-plane dispersion, between these samples (Figs. 4(b), 15(c), 24(b)). The results indicate that the crystallographic quality slightly degrades when deposited on an MgO single crystal with higher index plane.

Differences in coercivity are also noted between the epitaxial thin films. In-plane coercivity decreases with increasing the Si content for the epitaxial Fe-Si films grown on three kinds of crystallographic planes of MgO single-crystal substrates (Figs. 6(a), 19(a), 27(a)). When the coercivity is compared, lower values are observed in the order of samples prepared on MgO(001) < MgO(110) < MgO(111) for the compositional range of $x = 0 - 10$ at. %. The low coercivities of Fe-Si(001) epitaxial films are considered to be due to the high crystallographic quality of single-crystal with low dispersion.

In the present study, Fe-Si single crystal films of

$A2(100)$ orientation are obtained on MgO(100) substrate. The Fe-Si films prepared on MgO(110) substrate are epitaxial films of $A2(211)$ orientation with bi-crystalline structure, whereas the films formed on MgO(111) are epitaxial films of $A2(110)$ consisting of variants. By using these epitaxial thin films, it is possible to investigate the magnetic properties such as magnetostriction[18], damping constant, etc. in relation to the crystallographic orientation of Fe-Si magnetic material. The thin film growth technique can be applicable to the preparation of Fe-Si single-crystal films, for example, with $A2(110)$ by changing the substrate to GaAs(110) crystal[19].

4. Conclusion

Fe-Si alloy thin films are deposited on MgO single-crystal substrates of (001), (110), and (111) orientations at temperatures ranging between RT and 600 °C by varying the Si composition, x, from 0 to 10 at. %. The effects of composition and substrate orientation on the structure and the magnetic properties are investigated. Fe-Si(001) single-crystal films are formed on MgO(001) substrates. Fe-Si films epitaxially grown on MgO(110) substrates consist of two (211) variants whose orientations are rotated around the film normal by 180° each other. Fe-Si(110) films grow epitaxially on MgO(111) substrates with two-type variants, Nishiyama-Wasserman and Kurdjumov-Sachs relationships. The orientation dispersion of Fe-Si film decreases with decreasing the Si composition, with increasing the substrate temperature, and with decreasing the index of substrate crystallographic plane. The magnetic properties of films prepared on MgO(001) and (110) are reflecting the magnetocrystalline anisotropy of bulk Fe-Si crystal with $A2$ structure. The Fe-Si epitaxial films prepared on MgO(111) show almost isotropic in-plane magnetic anisotropies which are related with the multiple variant structure.

References

1) M. Takahashi, S. Suwabe, T. Narita, and T. Wakiyama: *J. Magn. Soc. Jpn.*, **10**, 307 (1986).
2) R. R. Rodriguez, G. A. Perez Alcazar, H. Sanchez, M. Sacilotti, and J. M. Greneche: *Phys. Status Solidi C*, **4**, 4220 (2007).
3) S. Yaegashi, T. Kurihara, and K. Satoh: *J. Magn. Soc. Jpn.*, **20**, 437 (1996).
4) L. T. Vinh, J. Chevrier, and J. Derrien: *Phys. Rev. B*, **46**, 946 (1992).
5) E. Schürmann, U. Hensgen: *Arch. Eisenhuettenwes*, **51**, 1 (1980).
6) M. Takahashi, Y. Takahashi, and H. Shoji: *IEEE Trans.*

Magn., **37**, 1937 (2001).

7) J. Waliszewski, L. Dobrzyńskia, A. Malinowskia, D. Satułaa, K. Szymańskia, W. Prandlb, Th Brückela, and O. Schärpf: *J. Magn. Magn. Mater.*, **132**, 349 (1994).

8) J. Yamashita and S. Asano: *J. Phys. Soc. Jpn.*, **52**, 3506 (1983).

9) F. C. Farquhar, H. Lipson, and A. R. Weill: *J. Iron Steel Inst.*, **152**, 457 (1945).

10) A. Nakamura, M. Koguchi, and M. Futamoto: *Jpn. J. Appl. Phys.*, **34**, 2307 (1995).

11) M. Ohtake, T. Nishiyama, K. Shikada, F. Kirino, and M. Futamoto: *J. Magn. Magn. Mater.*, **322**, 1947 (2010).

12) G. Wasserman: *Arch. Eisenhuettenwes*, **16**, 647 (1993).

13) Z. Nishiyama: *Sci. Rep. Tohoku Univ.*, **23**, 638 (1934).

14) G. Kurdjimov and G. Sachs: *Z. Phys.*, **64**, 325 (1930).

15) I. L. Grigorov, M. R. Fitzsimmons, I-Liang Siu, and J. C. Walker: *Phys. Rev. Lett.*, **82**, 5309 (1999).

16) Y. Asai, M. Ohtake, T. Kawai, and M. Futamoto: *J. Korean Phys. Soc.*, **63**, 733 (2013).

17) K. Matsubara, M. Ohtake, K. Tobari, and M. Futamoto: *Thin Solid Films*, **519**, 8299 (2011).

18) T. Kawai, T. Aida, M. Ohtake, and M. Futamoto: *J. Appl. Phys.*, **117**, 17A303 (2015).

19) M. W. Ruckman, J. J. Joyce, and J. H. Weaver: *Phys. Rev. B*, **33**, 7029 (1986).